ACS APPLIED NANO MATERIALS
Cite This: ACS Appl. Nano Mater. 2019, 2, 7421−7431
Article
www.acsanm.org

Sensitive and Specific Colorimetric Detection of Cancer Cells Based on Folate-Conjugated Gold−Iron-Oxide Composite Nanoparticles

Yun Teng

Department of Electrical and Electronic Engineering, The University of Hong Kong, Hong Kong

Jue Shi

Department of Physics, Hong Kong Baptist University, Hong Kong

Philip W. T. Pong*

Department of Electrical and Electronic Engineering, University of Hong Kong, Hong Kong

Supporting Information

ABSTRACT: A sensitive and specific colorimetric analytical strategy for cancer-cell detection based on folate-conjugated gold−iron-oxide composite nanoparticles (Au-Fe_2O_3 CNPs) has been developed. The synthesized Au-Fe_2O_3 CNPs demonstrated peroxidase-like activity and could catalyze the oxidation of 3,3′,5,5′-tetramethylbenzidine in the presence of the hydrogen peroxide. In this method, the Au-Fe_2O_3 CNPs were used as the signal transducer, and the conjugated folic acid acted as the cancer-cell recognition tool. The generated colorimetric signals could be detected by the naked eye or via a UV−vis spectrophotometer at an absorbance of 450 nm from the final yellow product. This folate-conjugated Au-Fe_2O_3 CNP-based colorimetric method allows the detection of cancer cells in the linear range from 50 to 500 cells/mL with a limit of detection of 5 cells/mL for the HeLa cells, which is much lower than that of other colorimetric detection methods for cancer cells. The specificity of this colorimetric detection method was indicated by both fluorescence microscopy images and UV−vis absorbance spectra. Moreover, the colorimetric detection of cancer cells in serum was performed to verify the feasibility of this colorimetric detection method in a complex biological environment. The folate-conjugated Au-Fe_2O_3 CNPs enabled the formation of a colorimetric-responsive multifunctional analysis platform with target recognition for cancer cell detection.

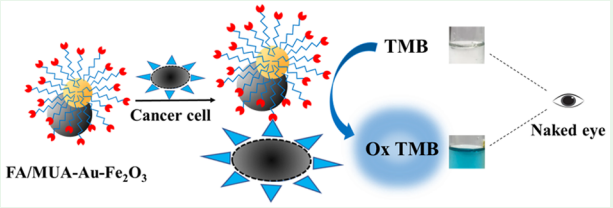

KEYWORDS: *gold−iron-oxide CNPs, peroxidase-like activity, colorimetric detection, folate and folate receptor, cancer cells*

1. INTRODUCTION

On the basis of the report from the World Health Cancer Organization, cancer has become a major public health problem worldwide, and it is the second leading cause of death, responsible for an estimated 9.6 million deaths in 2018.[1] Because of the late-stage presentation and inaccessible diagnosis and therapy of cancer, the rapid and efficient detection of cancer cells in preclinical stages would considerably improve the survival rate, reduce the mortality rate, decrease the cost of cancer diagnosis, and improve treatment timeliness.[2−4] Recently, a variety of cancer-cell detection methods based on different monitored signals have been developed, such as colorimetric detection,[5−7] fluorescence,[8−11] chemiluminescence,[12] and electrochemistry.[13−17] The colorimetric detection platform has attracted much attention because of its low cost, high feedback efficiency, and simple operation procedures.[18,19] Additionally, the colorimetric signal generated via the catalysis effect of natural enzymes including horseradish peroxidase (HRP) can be rapidly recognized by the naked eye.[20,21] However, the applications of natural enzymes are still limited by disadvantages including poor operational stability, long reaction time, and high preparation and purification costs. Therefore, enzyme-mimicking nanomaterials are ideal substitutes for colorimetric detection because of their easy preparation with controllable structure and size and desired catξalytic activity.[22,23]

A member of the nanoenzyme family, iron oxide nanoparticle (Fe_2O_3 NP)-based nanozymes have been receiving attention due to their enzyme mimetic specificity and electrochemical analysis capabilities.[24−28] However, the peroxidase-like catalytic process of Fe_2O_3 NP-based nanozymes usually presents low efficacy. It has been observed that appropriate design in terms of morphology and structure,

Received: October 8, 2019
Accepted: November 4, 2019
Published: November 4, 2019

DOI: 10.1021/acsanm.9b01947
ACS Appl. Nano Mater. 2019, 2, 7421−7431

crystal size modulation, and compositional regulation[29,30] can significantly enhance the functionality of iron-oxide nanozymes. A range of materials, such as graphene,[25,27] carbon dots,[24] polymers,[32] and oxides,[33] can form composites with Fe_2O_3 NPs to optimize the catalytic process. Gold nanoparticles (Au NPs) have become very useful nanomaterials in a biological science, primarily due to their biocompatibility, simple integration with biomolecules, and tunable optical properties.[31,32] Therefore, the combination of Fe_2O_3 NPs and Au NPs could be a scalable method of improving catalytic activity in colorimetric methods. Furthermore, because of the existence of specific biomarkers in cancer cells, the selective targeting mechanism based on specific recognition is of significant value to point-of-care cancer diagnosis and treatment applications. One of the cancer-specific antigens, alpha isoform folate receptor (FRα), also known as folate binding protein (FBP), is a glycosylphosphatidylinositol (GPI)-anchored membrane protein that can bind to and coordinate the transport of folate with high affinity.[33] Potocytosis is a traditional endocytotic trafficking process of folate through FRα.[34] The specific binding of FRα to folate creates a receptor−ligand complex; then, intracellular vesicles are formed after invagination and budding off. Once internalized, the uncoating and single vesicles formed early endosomes. These early endosomes were subsequently fused with lysosome after acidification. The process could assist in the dissociation of folate from FRα for the one-carbon metabolic reaction.[35] There are some reports that FRα is overexpressed in solid tumors such as breast carcinoma and ovarian cancer.[36] Thus the strong affinity between folate and folate receptors enables the targeted detection of cancer cells for the overexpression of FRα.[37−42]

Herein our research aims to develop a sensitive and specific colorimetric detection strategy to detect even small numbers of the cancer cells. We present a sensitive and specific colorimetric detection strategy for cancer cells based on folate-conjugated gold−iron-oxide composite (Au-Fe_2O_3) composite nanoparticles (CNPs). The Au-Fe_2O_3 CNPs were produced by a seed-mediated growth process in which the Fe_2O_3 NPs were used as the nucleation sites for the growth of Au NPs under mild reaction conditions. The synergistic Au-Fe_2O_3 CNPs exhibited favorable peroxidase-like activity. In this method, the Au-Fe_2O_3 CNPs acted as the signal transducer by catalyzing the oxidation of a colorless peroxidase substrate tetramethylbenzidine (TMB) in the presence of hydrogen peroxide (H_2O_2). Conjugated folic acid (FA) was applied as the cancer-cell recognition tool.[43,44] The generated colorimetric signals of the final yellow product could be rapidly recognized by the naked eye or via a UV−vis absorbance spectrophotometer. The limit of detection (LOD) of this FA/11-mercaptoundecanoic acid (MUA) Au-Fe_2O_3 (FA/MUA-Au-Fe_2O_3) CNP-based colorimetric detection platform is 5 cells/mL. The specificity of this colorimetric detection method was demonstrated by both fluorescence microscopy images and UV−vis absorbance spectra. Moreover, the colorimetric detection of cancer cells in serum was exploited to verify the feasibility of this colorimetric detection method in a complex biological environment. Finally, the cytotoxicity of this reported colorimetric detection method was also studied.

2. EXPERIMENTAL SECTION

2.1. Materials. Iron(III) oxyhydroxide (FeOOH), oleic acid (90%), and octadecene (90%) oleylamine were purchased from Sigma-Aldrich. Ethanol, hexanol, acetone, chloroform, toluene, and cyclohexane were obtained from Acros Organics. Chloroauric acid ($HAuCl_4$, 99%), 1,2-tetradecanediol, MUA, *N*-(3-(dimethylamino)-propyl)-*N*-ethylcarbodiimide hydrochloride (EDC, 99%), *N*-hydroxysuccinimide (NHS, 98%), doxorubicin hydrochloride (DOX, 98−102%), FA (97%), methyl thiazolyl tetrazolium (MTT), and dimethyl sulfoxide (DMSO) were purchased from Sigma. Dulbecco's modified Eagle's medium (DMEM), fluoroborate DMEM, fetal bovine serum (FBS), penicillin−streptomycin, and trypsin−EDTA were obtained from Life Technologies Limited. TMB was purchased from Neobioscience Technology. H_2O_2 and sulfuric acid (H_2SO_4) were obtained from International Laboratory. Glucose (Glu) and Hemoglobin (Hb) were purchased from J&K, and trace element solution (Tes) was purchased from Shanghai Guangyu Biological Technology. All chemicals were analytical grade and could be used without additional purification. All solutions were prepared in DI water or phosphate buffer saline (PBS).

2.2. Synthesis of Au-Fe_2O_3 CNPs. The monodisperse Fe_2O_3 NPs capped with oleylamine, and oleic acid were synthesized according to a reported method.[45] FeOOH (3 mmol) was dissolved in a mixture of oleic acid (2 mmol), oleylamine (6 mmol), and 1-octadecene (20 mL). The mixture was heated to 120 °C for 1 h and to 220 °C for 2 h with constant stirring and then refluxed at 300 °C for 1 h in the presence of nitrogen. The resulting solution was then cooled to room temperature, washed several times with acetone, and dispersed in chloroform. Monodisperse iron oxide Fe_2O_3 NPs capped with oleylamine were formed. Au-Fe_2O_3 CNPs were prepared based on an improved procedure from the literature.[46] $HAuCl_4$ (0.3 mmol) dissolved in oleylamine (6 mmol) was added dropwise to the toluene solution (20 mL) containing Fe_2O_3 NPs (0.45 mmol, based on Fe) and tetradecanediol (0.2 mmol). The solution was heated to 85 °C under a nitrogen atmosphere and maintained at this temperature for 8 h. After 8 h, the final products were washed several times and precipitated with ethanol. The Au-Fe_2O_3 CNPs were capped with oleylamine and dispersed in chloroform.

2.3. Preparation of FA/MUA-Au-Fe_2O_3 CNPs. The Au-Fe_2O_3 CNPs were modified with thiolated MUA through ligand exchange.[47] In brief, 2 mL of a 20 mM suspension of freshly prepared MUA was dissolved in ethanol and added to 10 mL of a 10 nM suspension of synthetic Au-Fe_2O_3 CNPs dispersed in chloroform. The mixture was vortexed for 5 min and incubated for 24 h. Then, the products were washed three times with anhydrous ethanol and centrifuged at 8000 rpm for 30 min to remove excess MUA. Subsequently, carboxyl-modified MUA-Au-Fe_2O_3 CNPs were covalently conjugated with FA via a typical EDC/NHS protocol. To activate the carboxylic groups (COOH) of MUA-Au-Fe_2O_3 CNPs, the MUA-Au-Fe_2O_3 CNPs were added to a solution of NHS (0.01 M) and EDC (2 mM) in PBS buffer and incubated for 30 min in a dark environment. Then, 2 mM FA was added to 10 mL of 2-(*N*-morpholino)ethanesulfonic acid (MES) buffer at room temperature. Then, the mixture was gently stirred in darkness for 24 h, and the resulting product was centrifuged and washed three times to obtain the filtrate. Finally, the FA/MUA-Au-Fe_2O_3 CNPs were resuspended in PBS buffer and stored at 4 °C.

2.4. Cell Culture and Detection of Cancer Cells. Human cervical cancer (HeLa) cells, human breast cancer (MCF-7) cells, and human dermal fibroblast (HDF) cells were maintained in DMEM supplemented with 10% FBS, 50 U/mL penicillin, and 50 μL/mL streptomycin. The cells were grown in a humidified incubator containing 5% CO_2 at 37 °C. The HeLa cells were suspended in PBS solution (10 mM, pH 7.4) at different concentrations.

To conduct the colorimetric detection assay, the cells were plated in 96-well plates at concentrations of 5000 cells/mL and allowed to adhere overnight; then, the cells were incubated with various densities of FA/MUA-Au-Fe_2O_3 CNPs for 1.5 h. MUA-Au-Fe_2O_3 CNPs and the normal human cells were employed as probe controls and cell controls, respectively, followed by the washing of every cell well with PBS solution (10 mM, pH 7.4) three times to eliminate unattached FA/MUA-Au-Fe_2O_3 CNPs. Subsequently, 200 μL of PBS solution (20 mM, pH 5.0) consisting of 0.8 mM TMB and 1 M H_2O_2 was added to each cell well, and the mixture was incubated at 45 °C for 10

DOI: 10.1021/acsanm.9b01947
ACS Appl. Nano Mater. 2019, 2, 7421−7431

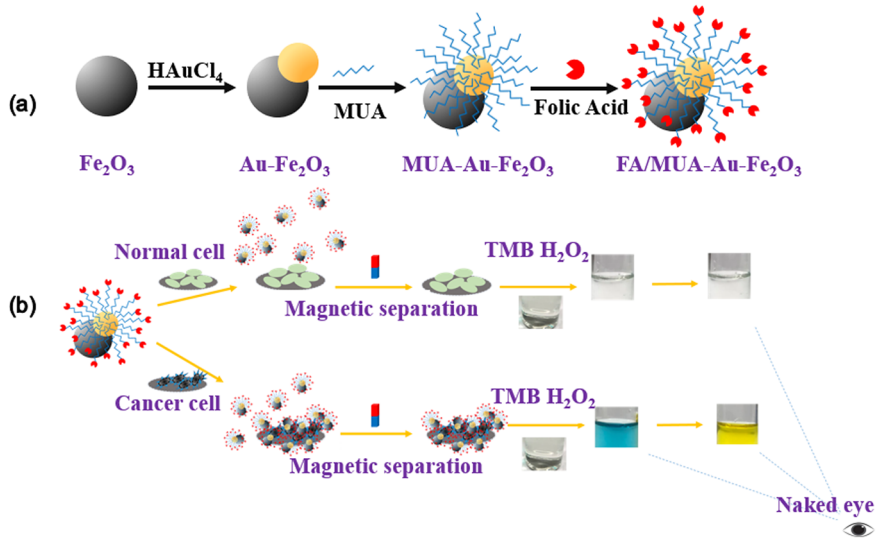

Figure 1. Schematic illustration of (a) the synthesis process of the FA/MUA-Au-Fe_2O_3 CNPs and (b) the working principle of the FA/MUA-Au-Fe_2O_3 CNP-based colorimetric detection method for the target cancer cells.

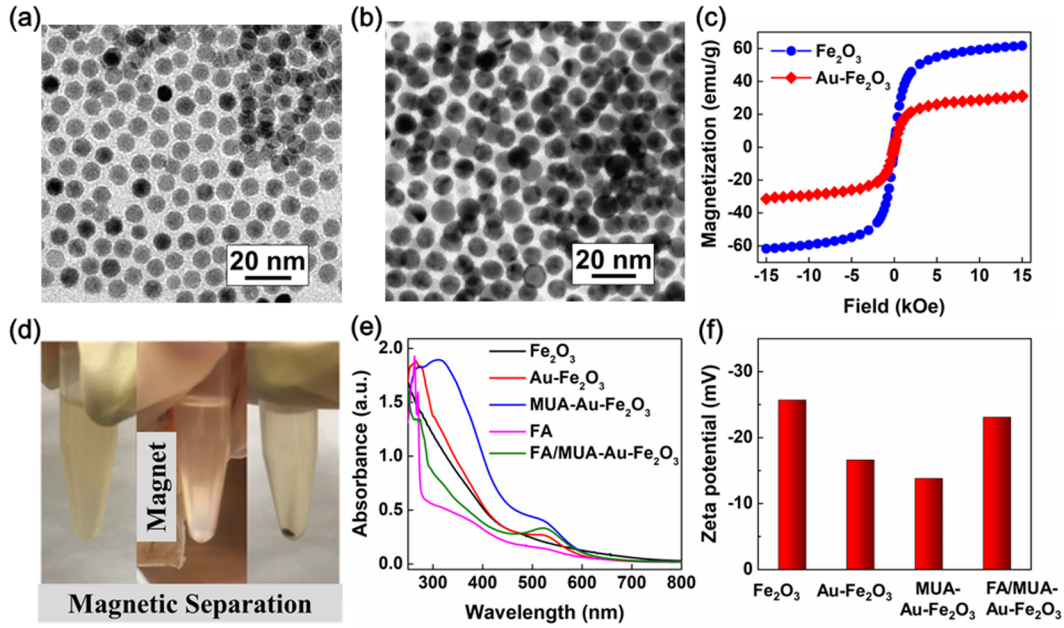

Figure 2. TEM images of (a) Fe_2O_3 NPs and (b) Au-Fe_2O_3 CNPs, (c) VSM curves of Fe_2O_3 NPs and Au-Fe_2O_3 CNPs, (d) photographs of Au-Fe_2O_3 CNPs before and after magnetic separation, (e) UV−vis spectra of Fe_2O_3, Au-Fe_2O_3, MUA-Au-Fe_2O_3, FA, and FA/MUA-AuFe_2O_3 CNPs, and (f) ξ potential of Fe_2O_3, Au-Fe_2O_3, MUA-Au-Fe_2O_3, and FA/MUA-Au-Fe_2O_3 CNPs.

min. Finally, H_2SO_4 (1 M) was used to stop the reaction, and a microplate reader was used to quantitatively monitor the absorbance at a wavelength of 450 nm. Various cell concentrations, including 50, 100, 300, 400, 500, 1000, 3000, 5000, and 10 000 cells/mL, were used to analyze the target cells quantitatively. To detect the cells in serum, the cell samples were prepared by diluting FBS with PBS buffer at a ratio of 1:24. The interferent samples were prepared in PBS buffer at the same ratio 1:24 (volume/volume).

2.5. Characterization. The morphologies of the as-prepared CNPs were characterized by a Philips CM-100 transmission electron microscope (TEM) operating at 100 kV. The structures of the CNPs were examined by a LEO 1530 scanning electron microscope (SEM). The magnetic characterization of the CNPs was carried out with a MicroSense EZ vibrating sample magnetometer (VSM) at 300 K. The investigation of the size and surface charge (zeta (ξ) potential) of the CNPs was achieved by dynamic light scattering (DLS) on a Zetasizer Nano ZS instrument (Malvern Instruments, U.K.). UV−vis spectra were measured from a UV/visible spectrophotometer (Agilent Cary 60). Colorimetric signals and cell cytotoxicity data were collected using a microplate reader (Molecular Devices VERSA max microplate reader) at 450 and 490 nm, respectively. The fluorescence spectrum of the CNPs was obtained using a spectrofluorometer (Edinburgh FLSP920). The fluorescence images were obtained from a confocal laser scanning microscope (Carl Zeiss LSM710).

3. RESULTS AND DISCUSSION

3.1. Principle of the FA/MUA-Au-Fe_2O_3 CNP-Based Colorimetric Detection of Cancer Cells. The process of synthesizing the FA/MUA-Au-Fe_2O_3 CNPs is illustrated in Figure 1a. The carboxyl group modified by the Au-Fe_2O_3 CNPs was conjugated with FA through covalent bonding. The

DOI: 10.1021/acsanm.9b01947
ACS Appl. Nano Mater. 2019, 2, 7421−7431

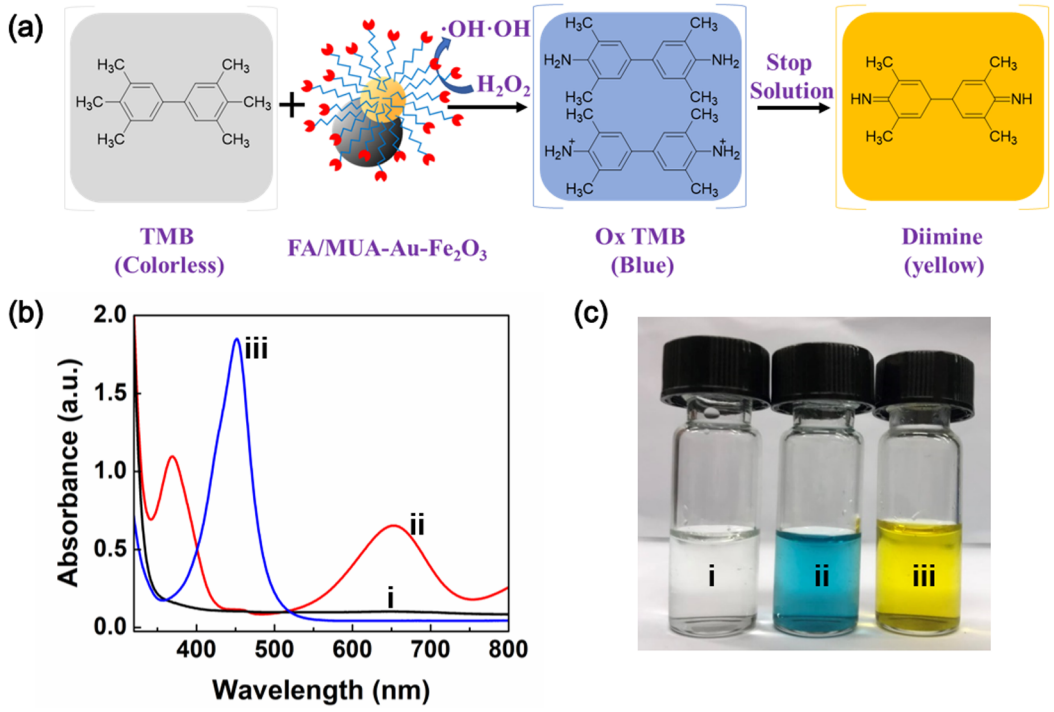

Figure 3. (a) Mechanism of the peroxidase-like activity of the FA/MUA-Au-Fe_2O_3 CNPs for the oxidation of TMB in the presence of H_2O_2, (b) UV−vis spectra, and (c) photographs of the catalyzed reaction solution containing TMB and H_2O_2 (i) in the absence of the FA/MUA-Au-Fe_2O_3 CNPs, (ii) in the presence of the FA/MUA-Au-Fe_2O_3 CNPs, and (iii) after quenching by H_2SO_4.

fabricated Au-Fe_2O_3 CNPs exhibited peroxidase-like activity, which could catalyze the oxidation of TMB in the presence of H_2O_2, and the conjugated FA could be used as the cancer-cell recognition tool. As shown in Figure 1b, after incubation with the cancer cells, the folate-conjugated FA/MUA-Au-Fe_2O_3 CNPs were trapped on the membrane of the cancer cells due to the strong affinity between the FA and the specific folate receptor (FR) in the cell membrane. After separating the unattached NPs with a magnet, the generated colorimetric signals could be distinguished by the naked eye (the color of the solution changed from blue to yellow) or the UV−vis absorbance spectrophotometer at 450 nm. In contrast, there was no color change in the group incubated with the normal cells.

3.2. Synthesis and Characterization of the Folate-Conjugated Au-Fe_2O_3 CNPs. The Fe_2O_3 NPs were synthesized by a thermal decomposition protocol. Figure 2a shows that the Fe_2O_3 NPs capped with oleylamine and oleic acid are spherical, with an average size of 9.8 ± 0.7 nm. The Au-Fe_2O_3 CNPs were produced by the seed-mediated growth process, and the Fe_2O_3 NPs were used as the nucleation sites for the growth of Au NPs. The Au-Fe_2O_3 CNPs were well-dispersed with an average size of 12.4 ± 1.9 nm, as shown in Figure 2b. The addition of the Au precursor and oleylamine increased the diameter of the Fe_2O_3 NPs, resulting in the spherical morphology of the Au-Fe_2O_3 CNPs. The energy-dispersive X-ray (EDX) spectrum and elemental composition analysis of the Au-Fe_2O_3 CNPs confirmed the existence of C, O, Si, Fe, and Au. The Au peak was attributed to the synthesized Au-Fe_2O_3 CNPs (Figure S1). The magnetization (MH) curve of the Au-Fe_2O_3 CNPs and Fe_2O_3 NPs was measured at room temperature. The Fe_2O_3 NPs before the growth of Au exhibited a low coercivity *Hc* of 0.9 Oe (Figure 2c), demonstrating the superparamagnetic property of the Fe_2O_3 NPs. The coercivity of the Au-Fe_2O_3 CNPs increased to 4.9 Oe because of the Au metal seeded on the Fe_2O_3 NPs, leading to larger CNPs and less effective coupling of magnetic dipole moments.[48] The magnetization of the Fe_2O_3 NPs was 61.7 emu/g, whereas that of the Au-Fe_2O_3 CNPs was 30.8 emu/g. The decrease in the specific saturation magnetization was attributed to the nonmagnetic Au metal in the CNPs. Although the magnetization of FA/MUA-Au-Fe_2O_3 CNPs decreased, it was still strong enough to allow the effective separation of the FA/MUA-Au-Fe_2O_3 CNPs from the unattached NPs using a magnet in 5 min, as presented in Figure 2d. The UV−visible experiment was performed to characterize the modification of the fabricated NPs. As shown in Figure 2e, the Fe_2O_3 NPs did not have a distinct absorption peak. The Au-Fe_2O_3 CNPs exhibited a heavy absorption peak at 523 nm, reflecting the prominent optical properties of the CNPs. The right shift of the absorption peak of pure Au NPs (~517 nm) may be attributed to the increased size of the Au NPs and the insufficient electron population on Au caused by the interfacial connection between Au and Fe_2O_3 NPs.[49−51] Additionally, FA showed a characteristic absorption peak at ~280 nm. After being modified with MUA and conjugated with FA, the absorption spectra of the obtained FA/MUA-Au-Fe_2O_3 CNPs showed the characteristic peaks of both Au and FA at 520 and 278 nm, respectively, indicating the successful formation of FA/MUA-Au-Fe_2O_3 CNPs. Furthermore, the ξ potential measurement was used to characterize the conjugation between the FA and Au-Fe_2O_3 CNPs (Figure 2f). The ξ potential value of the MUA-Au-Fe_2O_3 CNPs was near −13.8 mV due to the deprotonation of the COOH group of the modified MUA, whereas the ξ potential of the FA/MUA-Au-Fe_2O_3 CNPs was −23.1 mV after conjugation. This change of ξ potential can be attributed to the electrostatic coupling

DOI: 10.1021/acsanm.9b01947
ACS Appl. Nano Mater. 2019, 2, 7421−7431

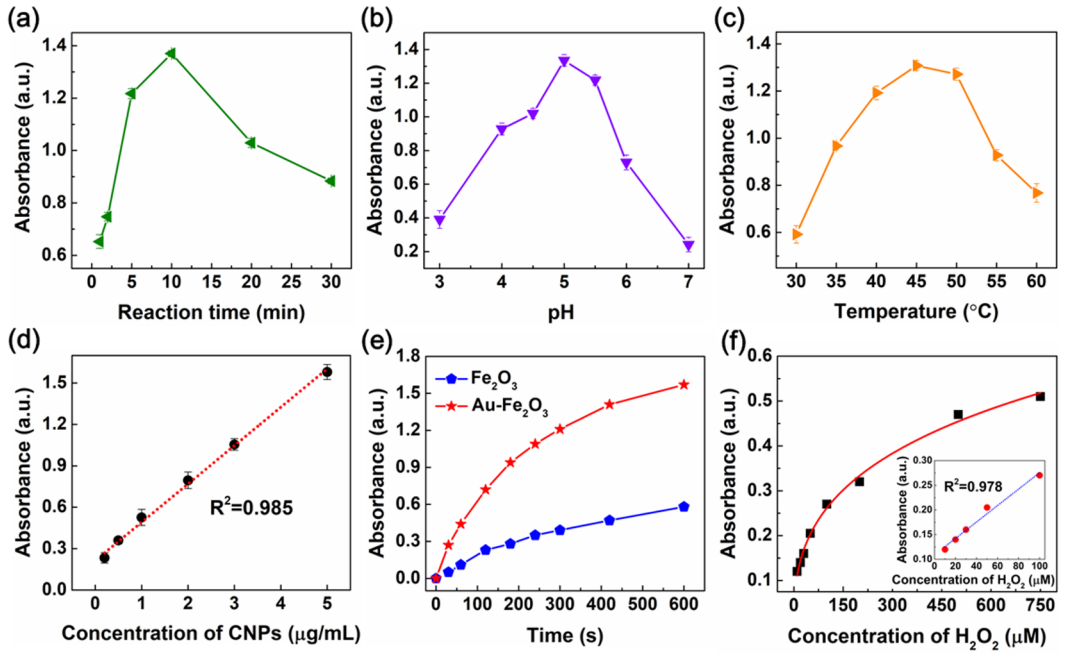

Figure 4. Effect of different experimental conditions on the catalytic activity of the FA/MUA-Au-Fe_2O_3 CNPs: (a) reaction time, (b) pH, (c) temperature, (d) CNP concentration, (e) comparison of Fe_2O_3 and Au-Fe_2O_3 CNPs, and (f) H_2O_2 concentration.

between the negatively charged −COOH and the positively charged $-NH_2$ in the FA molecules.

3.3. Peroxidase-Like Activity of the FA/MUA-Au-Fe_2O_3 CNPs. The characterization of the peroxidase-like activity of FA/MUA-Au-Fe_2O_3 CNPs was performed with peroxidase substrate TMB and H_2O_2. Figure 3a shows the mechanism of the peroxidase-like activity of FA/MUA-Au-Fe_2O_3 CNPs for the oxidation of TMB in the presence of H_2O_2. As displayed in Figure 3b,c, no visible color change was observed in the absence of FA/MUA-Au-Fe_2O_3 CNPs, indicating that there was no oxidation reaction of TMB. In contrast, FA/MUA-Au-Fe_2O_3 CNPs could catalyze the oxidation of TMB in the presence of H_2O_2, which could produce a blue product with maximum UV absorbances at 652 and 370 nm, as shown in Figure 3b. After adding H_2SO_4 to stop the catalytic reaction, the color of the solution changed from blue to yellow, and the final product presented a maximum absorption wavelength of 450 nm. These results confirmed the peroxidase-like activity of the FA/MUA-Au-Fe_2O_3 CNPs.

3.4. Optimization of Experimental Conditions for the Colorimetric Response of the FA/MUA-Au-Fe_2O_3 CNPs. The peroxidase-like activity was critical for the FA/MUA-Au-Fe_2O_3 CNP-based detection platform. The experimental parameters, including the reaction time, pH value, temperature, and concentration of fabricated NPs, were explored to achieve an optimal colorimetric effect on cancer-cell detection. The absorbance peak of TMB at 450 nm increased with the incubation duration up to 10 min and then decreased, as plotted in Figure 4a. Thus 10 min was the optimal time for the colorimetric reaction. The effect of reaction pH on the catalytic activity of the FA/MUA-Au-Fe_2O_3 CNPs is demonstrated in Figure 4b. The highest catalytic activity of the FA/MUA-Au-Fe_2O_3 CNPs was exhibited at pH 5. Although the catalytic activity of the FA/MUA-Au-Fe_2O_3 CNPs gradually increased with temperature (Figure 4c), a floc appeared in the reaction solution when the temperature was higher than 65 °C due to overoxidation. The optimal temperature for colorimetric experiments of this platform was chosen to be 45 °C. Figure 4d shows the relationship between the absorbance of the TMB oxidized product at 450 nm and the concentration of FA/MUA-Au-Fe_2O_3 CNPs. A dramatic enhancement in the catalytic rate was observed with the steady increase in the FA/MUA-Au-Fe_2O_3 CNP concentration.

The control experiment of pure Fe_2O_3 NPs has been carried out to verify the enhanced peroxidase-like catalytic activity of the Au-Fe_2O_3 CNPs. The peroxidase-like activity of FA/MUA-Au-Fe_2O_3 was monitored through a colorimetric reaction using TMB as substrates in the presence of H_2O_2. Figure 4e shows the time-dependent absorbance changes with the CNP, Fe_2O_3 NPs and Au-Fe_2O_3, as catalysts, respectively. The absorbance value of the substrate oxidation products represented the relative peroxidase-like activity. At the same iron concentration, Au-Fe_2O_3 NPs exhibited enhanced peroxidase-like activity compared with the Fe_2O_3 NPs. These results demonstrated that the peroxidase-like activity was greatly enhanced by integrating Au NPs and Fe_2O_3 NPs into one entity, in which the Fe_2O_3 NPs acted as enzyme-like catalytic centers and Au NPs played an important role in the enhancement of the catalytic activity. The optimal concentration of H_2O_2 for the colorimetric response has been investigated in the catalytic process. Figure 4f shows a typical H_2O_2 concentration−response curve in an acetate buffer solution (pH 5.5) by monitoring the absorbance changes with time. It is found that the absorbance increased with increasing H_2O_2 concentration. As demonstrated in the calibration plot in the inset of Figure 4f, the calculated LOD for H_2O_2 was ∼2.0 μM with a linear range from 10 to 100 μM (R^2 = 0.978). The LOD for H_2O_2 was determined on the basis of three times the standard deviation of the blank measurement.

3.5. Feasibility of the FA/MUA-Au-Fe_2O_3 CNP-Based Colorimetric Detection of Cancer Cells. To demonstrate the application performance of the FA/MUA-Au-Fe_2O_3 CNP-

DOI: 10.1021/acsanm.9b01947
ACS Appl. Nano Mater. 2019, 2, 7421−7431

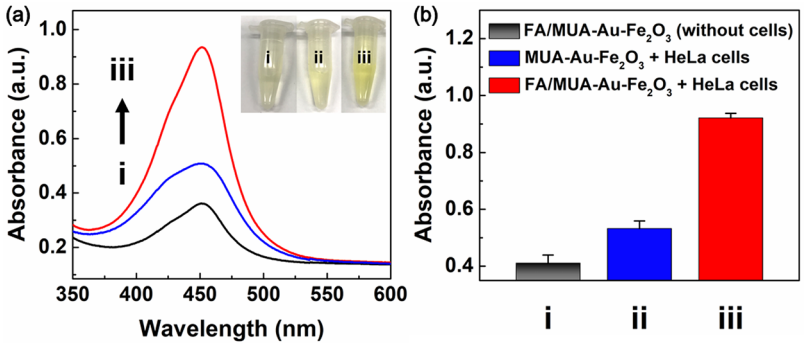

Figure 5. Feasibility investigation of the FA/MUA-Au-Fe_2O_3 CNP-based nanoprobe for cancer-cell detection: (a) photographs of different samples and UV−vis absorption spectra characterization and (b) histogram of absorbances at 450 nm: (i) the FA/MUA-Au-Fe_2O_3 CNPs incubated without the cells, (ii) the MUA-Au-Fe_2O_3 CNPs incubated with the HeLa cells, and (iii) the FA/MUA-Au-Fe_2O_3 CNPs incubated with the HeLa cells. (Data are displayed as the mean ± SD with n = 3.)

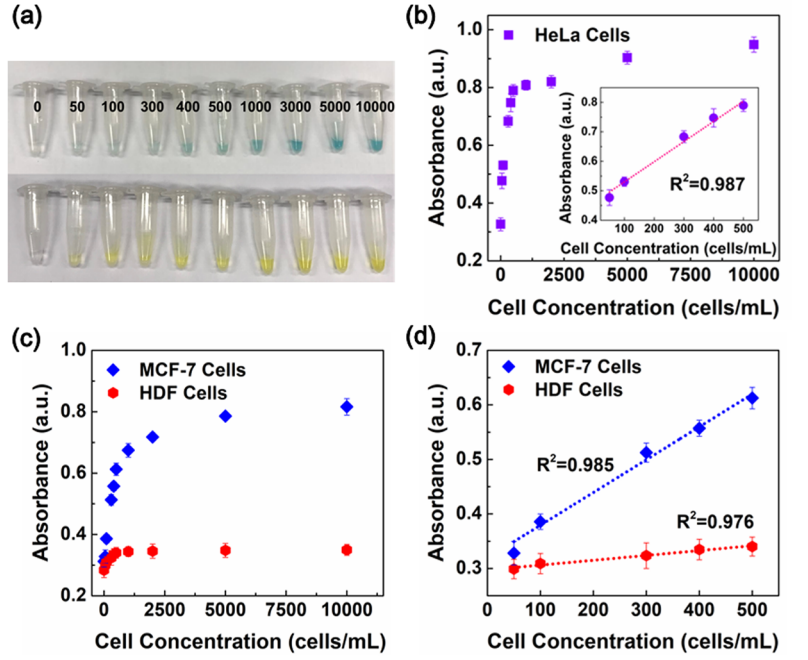

Figure 6. Quantitative analysis of the FA/MUA-Au-Fe_2O_3 CNP-based nanoprobe for the detection of cancer cells: (a) photographs for cancer-cell detection with the colorimetric method developed using the FA/MUA-Au-Fe_2O_3 CNP based on samples with different concentrations of the HeLa cells (0, 50, 100, 300, 400, 500, 1000, 3000, 5000, and 10000 cells/mL), (b) UV−vis absorbance at 450 nm as a function of the HeLa cell concentration (inset: linear calibration plot at low cell concentrations), (c) UV−vis absorbance at 450 nm as a function of the cell concentration, and (d) linear calibration curves on samples of MCF-7 and the HDF cells.

based colorimetric detection of cancer cells, the HeLa cells and the FA were selected as the target cells and the recognition tool in the detection process, respectively. In this work, the FA was modified with the Au-Fe_2O_3 CNPs through the EDC/NHS reaction to form the folate-conjugated FA/MUA-Au-Fe_2O_3 nanoprobe. The MUA-Au-Fe_2O_3 CNPs (without FA conjugation) were applied as the control probe, and the FA/MUA-Au-Fe_2O_3 CNPs incubated without the HeLa cells acted as the blank.

As presented in Figure 5a, the photograph of the visible yellow products could be recognized by the naked eye, whereas the group of the FA/MUA-Au-Fe_2O_3 CNPs incubated with the HeLa cells displayed increased absorption at 450 nm (Figure 5b). The results indicated that the selective binding of the FA/MUA-Au-Fe_2O_3 CNPs to the target cells was achieved via the interaction between FA and the FR, resulting in the assembly of the FA/MUA-Au-Fe_2O_3 CNPs around the target cells and the catalysis of the oxidation of TMB by H_2O_2.

3.6. Colorimetric Detection of Cancer Cells Based on FA/MUA-Au-Fe_2O_3 CNPs. To investigate the sensitivity and confirm the detection scope of this colorimetric cancer-cell detection platform, a variety of cell samples were prepared and then detected. Photographs of samples with densities ranging from 0 to 1.0 × 10^4 cells/mL in the TMB-H_2O_2 solution before and after adding H_2SO_4 to stop the catalyst reaction are displayed in Figure 6a. The solution color gradually becomes deeper with increasing cancer-cell concentration for both the blue products from the oxidization of TMB and the yellow products after adding H_2SO_4.

Except for the visual analysis, the sensitivity and detection range of this detection platform were also evaluated by quantitatively scaling the absorbance of the cell samples to 450

DOI: 10.1021/acsanm.9b01947
ACS Appl. Nano Mater. 2019, 2, 7421−7431

Table 1. Comparison of Colorimetric Methods for Cancer-Cell Detection

nanocomposite	method	cancer cell	limit of detection (cells/mL)	ref
folate-conjugated Au-Fe_2O_3 nanoparticles	peroxidase-like catalyzed TMB-H_2O_2 reaction	HeLa cells	5	this work
iodide-responsive Cu−Au nanoparticles	iodide-catalyzed TMB-H_2O_2 reaction	CCRF-CEM cells	50	53
multifunctional oval-shaped gold-NP-based nanoconjugate	peroxidase-like catalyzed TMB-H_2O_2 reaction	SKBR3 cells	100	54
porous Pt nanoparticles on graphene oxide	peroxidase-like catalyzed TMB-H_2O_2 reaction	MCF-7 cells	150	39
DNAzyme	peroxidase-like catalyzed TMB-H_2O_2 reaction	CCRF-CEM cells	500	55
spherical Au nanoparticles	distance-dependent optical properties	CCRF-CEM cells	660	56
incorporating graphene oxide and gold nanoclusters	peroxidase-like catalyzed TMB-H_2O_2 reaction	MCF-7 cells	1000	57

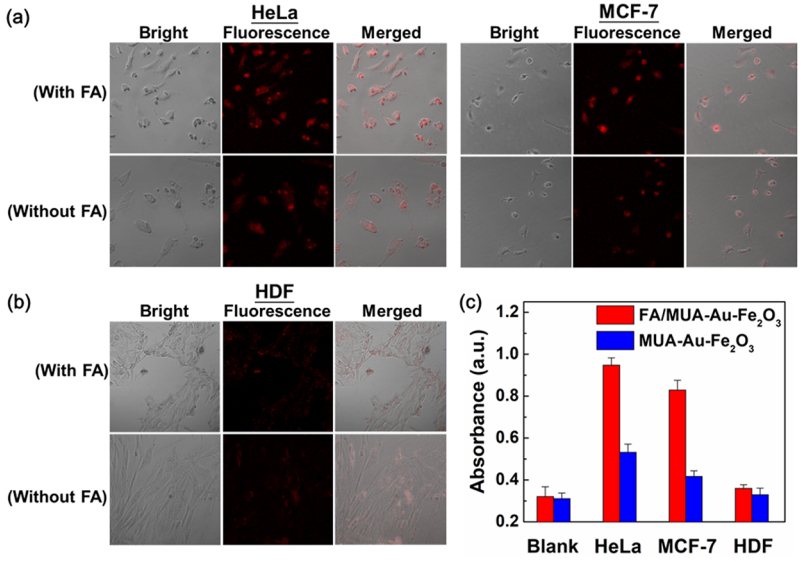

Figure 7. Targeting effect of the FA/MUA-Au-Fe_2O_3 CNP-based colorimetric detection for cancer cells and noncancerous cells indicated by fluorescence microscopy images: (a) HeLa cells and the MCF-7 cells and (b) HDF cells. (c) UV−vis absorbance spectra with and without FA CNPs groups for different samples. (data are displayed as the mean ± SD with n = 3.)

nm, as shown in Figure 6b. The UV−vis absorbance was linearly correlated with the cell concentrations from 50 to 500 cells/mL (R^2 = 0.987). This LOD is determined by the standard deviation method.[52] The LOD was calculated on the basis of three times the standard deviation of the blank measurement using the following equation

$$\text{limit of detection} = 3\sigma/k$$

where σ is the standard deviation of blank measurements and k is the slope of the plot of UV−vis absorbance at 450 nm as a function of the HeLa cell concentration. The LOD for HeLa cells was determined on the basis of three times the standard deviation of the blank measurement, which was calculated to be five cells; the smallest readily detected cell number with the naked eye was five cells in 1 mL of solution in real experiments under optimal experimental conditions, which is much lower than the LODs for the existing colorimetric cancer-cell detection methods (Table 1).[39,53−57]

To further confirm the sensitivity of this colorimetric assay for cancer detection, the same experiment was carried out on the other samples of the MCF-7 cells and the HDF cells. The HeLa cell and MCF-7 cells were the cancerous cells with the overexpression of FRα,[36] which could be specifically detected via the strong affinity between the folate of the modified Au-Fe_2O_3 CNPs and the folate receptors on the surface of the HeLa and MCF-7 cells.[37−40] In contrast, the HDF cells were the normal cells without the overexpression of the FR and thus acted as the control group. Compared with the cancer-cell groups, there was little difference in the absorbance of the normal cell group with the same concentration. The UV−vis absorption spectra and calibration curves of the FA/MUA-Au-Fe_2O_3 CNP-based colorimetric detection of the MCF-7 cells and the HDF cells were obtained, as shown in Figure 6c,d. The colorimetric signals of the cancer cells (MCF-7 cells) were significantly higher than those of the HDF cells due to the attachment of the FA/MUA-Au-Fe_2O_3 CNPs to the MCF-7 cells with the overexpression of the FR but not the HDF cells with no overexpression of the FR. Referring to the calculation of the LOD for HeLa cells, the LODs for HDF and MCF-7 were also determined by the standard deviation method, which was calculated on the basis of three times the standard deviation of the blank measurement. The LOD for MCF-7 cancer cells was calculated to be 27 cells, whereas the LOD for HDF noncancer cells was calculated to be 103 cells. The calculation results are in good agreement with the experimental results. These results suggested that the Au-Fe_2O_3 CNP-based colorimetric detection method is selective for the cancer cells.

DOI: 10.1021/acsanm.9b01947
ACS Appl. Nano Mater. 2019, 2, 7421−7431

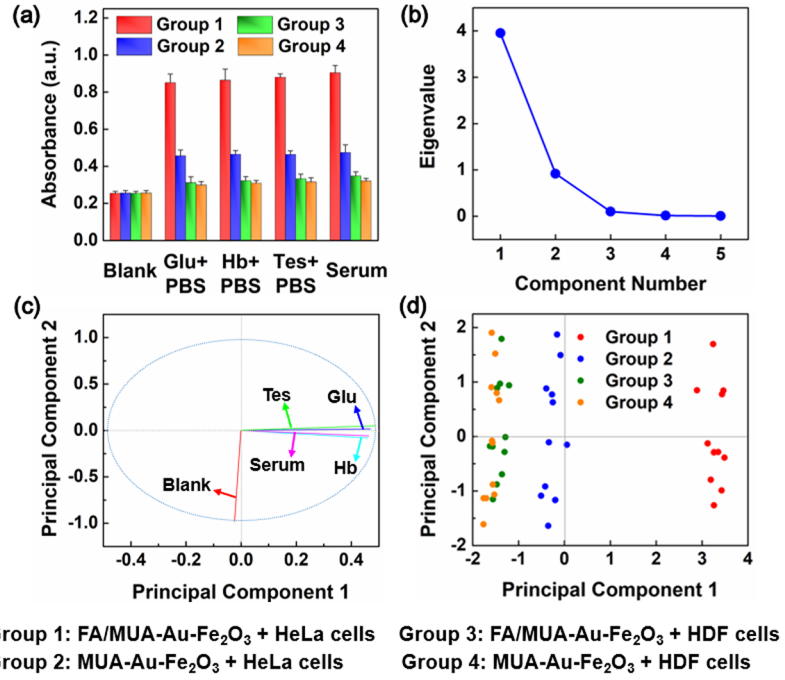

Figure 8. (a) UV−vis absorbance of the FA/MUA-Au-Fe_2O_3 CNP-based colorimetric detection of target cancer cells in diluted serum with different interferent samples. Principal component analysis (PCA) of serum sample and different interferent samples: (b) scree plots of the eigenvalues for the first five principal components (PCs), (c) loading plots of variables for the first two PCs, and (d) score plots of the serum sample and different interferent samples for the first two PCs. (Data are displayed as the mean ± SD with n = 3.)

3.7. Targeting Effect of the FA/MUA-Au-Fe_2O_3 CNP-Based Colorimetric Detection of Cancer Cells. Next, the targeting effect of the FA/MUA-Au-Fe_2O_3 CNP-based colorimetric detection method for cancer cells was analyzed by both fluorescence microscopic images and UV−vis absorbance spectra. The fluorescence emission of the Au-Fe_2O_3 CNPs is related to the surface adsorbate.[58] When being excited at 485 nm, the fluorescence emission peak located at 618 nm displays red photoluminescence (Figure S2). Therefore, fluorescence microscopy was used to verify that the FA/MUA-Au-Fe_2O_3 CNPs were assembled on the surface of the target cells and to visualize the targeting effect of the FA/MUA-Au-Fe_2O_3 CNPs toward the HeLa and MCF-7 cancer cells using the red fluorescence of the Au-Fe_2O_3 CNPs. In this experiment, the HeLa and MCF-7 cells were selected as the target groups with an overexpression of the FR, whereas the HDF cells with the absence of an FR served as the control group. After incubation for 1.5 h, a clear visualization of red fluorescence was observed for the HeLa and MCF-7 cells (Figure 7a), whereas no obvious fluorescence was seen from the HDF cells (Figure 7b), signifying the specific targeting ability of CNPs to the HeLa and MCF-7 cancer cells through the FA targeting ligand. The target cancer-cell groups showed a higher absorbance at 450 nm than the control group incubated with the normal cells, as presented in Figure 7c. The cancer cells incubated with the MUA-Au-Fe_2O_3 CNPs exhibited a weak colorimetric response signals due to the simple passive diffusion of the MUA-Au-Fe_2O_3 CNPs entering the cancer cells.[59] These results showed that the FA-conjugated CNPs could enter into the HeLa and MCF-7 cancer cells overexpressed with the FR, whereas much fewer CNPs entered the HDF cells due to the absence of an FR on the noncancerous cells. Additionally, more FA/MUA-Au-Fe_2O_3 CNPs were bound to the HeLa cells than to the MCF-7 cells because the HeLa cells have more FR expression on their cell membranes. Therefore, this FA/MUA-Au-Fe_2O_3 CNP-based colorimetric detection method could become a general platform for cancer-cell detection because the FR is overexpressed in the cell membranes of a range of cancer cells, such as ovarian, colorectal, and breast cancers.[60]

3.8. Principal Component Analysis for the FA/MUA-Au-Fe_2O_3 CNP-Based Colorimetric Detection of Cancer Cells. Additionally, the application of this colorimetric strategy for cancer-cell detection in serum was explored. The as-prepared FA-conjugated CNPs and CNPs without FA conjugation were applied in diluted serum, and other interferent samples with the cancer cells (HeLa cells), the noncancerous cells (HDF cell), and no cells served as blanks. The colorimetric signals were quantitatively measured and analyzed via the absorbance at 450 nm. As shown in Figure 8a, the absorbance induced by the group of the FA-conjugated CNPs incubated with the HeLa cells was higher than that without FA. In contrast, there was a negligible influence on the normal HDF cells. To verify the ability of colorimetric signals to distinguish the cancer cells and the noncancerous cells in different interferent samples, principal component analysis (PCA) was performed on the measured UV−vis spectra with SPSS software. PCA is a statistical technique used to simplify complex data sets and explain the variation in the data using linear combinations of multiple variables. Principal components (PCs) are usually displayed in decreasing order of importance when explaining the variability in the data matrix. As presented in Figure 8b, the scree plot for the colorimetric signals (UV−vis data set) showed the size of the eigenvalues for the first five PCs, and the first two PCs explained ~97% of the variation in the data. Figure 8c shows the loading plots of the different variables for PC1 and PC2, which notes the close covariation of the interferent groups and the serum group. For

DOI: 10.1021/acsanm.9b01947
ACS Appl. Nano Mater. 2019, 2, 7421−7431

PC1, which contrasted sharply with PC2, the loading values were very close to positive values (except for the blank group), as expected due to their similar relationship to colorimetric signals. The score plots of PC2 against PC1 are shown in Figure 8d, where the different colors represent different groups. The results noted the clear separation of the two groups of the HeLa cells, indicating the targeting effect of the conjugated FA for the cancer cells. For the noncancerous cells, there was no clear separation attributed to the absence of an FR. The experimental results revealed that the FA/MUA-Au-Fe_2O_3 CNP-based cancer-cell detection strategy is feasible and sensitive in a complex biological environment, which paves the way for future clinical therapy applications. Finally, the cytotoxicity of the FA/MUA-Au-Fe_2O_3 CNPs was studied by an MTT assay, as presented in Figure S3. After incubation with various FA/MUA-Au-Fe_2O_3 CNPs, with the concentration from 0 to 50 μg/mL for 1.5 h, the relative survival rate of the HeLa cells was 99.68%. The survival rate remained 90% even after 24 h, proving that the FA/MUA-Au-Fe_2O_3 CNPs were not cytotoxic to the cancer cells.

4. CONCLUSIONS

This Article reports a sensitive and specific colorimetric detection strategy based on folate-conjugated Au-Fe_2O_3 CNPs for cancer-cell detection. The Au-Fe_2O_3 CNPs were obtained by the seed-mediated growth protocol in which Fe_2O_3 NPs were used as the nucleation sites for the growth of Au NPs under mild reaction conditions. The fabricated Au-Fe_2O_3 CNPs showed peroxidase-like activity, and the conjugated FA on the Au-Fe_2O_3 CNPs was used as the recognition tool. The FA/MUA-Au-Fe_2O_3 CNP-based colorimetric detection strategy for cancer cells successfully achieved the simple and sensitive detection of cancer cells in the linear range from 50 to 500 cells/mL, with the LOD for the HeLa cells of 5 cells/mL. The specificity of this colorimetric detection method was analyzed by both fluorescence microscopic images and UV−vis absorbance spectra. Moreover, the experiments of the cancer-cell assay were conducted in diluted serum solutions to indicate the feasibility of this colorimetric detection method in a complex biological environment. Therefore, the folate-conjugated colorimetric-responsive target-recognizing Au-Fe_2O_3 composite nanoprobe can be used as a powerful tool for future clinical cancer diagnosis.

■ ASSOCIATED CONTENT

Supporting Information

The Supporting Information is available free of charge on the ACS Publications website at DOI: 10.1021/acsanm.9b01947.

EDX measurement and elemental analysis of Au-Fe_2O_3 CNPs, fluorescence spectrum of the FA/MUA-Au-Fe_2O_3 CNPs, and cytotoxicity of the FA/MUA-Au-Fe_2O_3 CNPs (PDF)

■ AUTHOR INFORMATION

Corresponding Author

*Tel./Fax: +852 2857 8491. E-mail: ppong@eee.hku.hk.

ORCID

Yun Teng: 0000-0002-7826-751X

Notes

The authors declare no competing financial interest.

■ ACKNOWLEDGMENTS

This research was supported by the Seed Funding Program for Basic Research, Seed Funding Program for Applied Research and Small Project Funding Program from University of Hong Kong, ITF Tier 3 funding (ITS-104/13, ITS-214/14), and University Grants Committee of Hong Kong (AoE/P-04/08). J.S. (HKBU) acknowledges the support by the Research Grant Council of Hong Kong (C2006-17E and T12-710/16-R). Helen Leung (HKU) is thanked for confocal microscope measurements.

■ REFERENCES

(1) Bray, F.; Ferlay, J.; Soerjomataram, I.; Siegel, R. L.; Torre, L. A.; Jemal, A. Global cancer statistics 2018: GLOBOCAN estimates of incidence and mortality worldwide for 36 cancers in 185 countries. *Ca-Cancer J. Clin.* **2018**, *68* (6), 394−424.

(2) Uhr, J. W. Cancer diagnostics: one-stop shop. *Nature* **2007**, *450* (7173), 1168−9.

(3) Ebert, M. P.; Korc, M.; Malfertheiner, P.; Rocken, C. Advances, challenges, and limitations in serum-proteome-based cancer diagnosis. *J. Proteome Res.* **2006**, *5* (1), 19−25.

(4) Savage, N. Early detection: Spotting the first signs. *Nature* **2011**, *471* (7339), S14−5.

(5) Chen, C.; Song, G.; Ren, J.; Qu, X. A simple and sensitive colorimetric pH meter based on DNA conformational switch and gold nanoparticle aggregation. *Chem. Commun. (Cambridge, U. K.)* **2008**, No. 46, 6149−51.

(6) Medley, C. D.; Smith, J. E.; Tang, Z.; Wu, Y.; Bamrungsap, S.; Tan, W. Gold nanoparticle-based colorimetric assay for the direct detection of cancerous cells. *Anal. Chem.* **2008**, *80* (4), 1067−72.

(7) Wang, K.; Fan, D.; Liu, Y.; Wang, E. Highly sensitive and specific colorimetric detection of cancer cells via dual-aptamer target binding strategy. *Biosens. Bioelectron.* **2015**, *73*, 1−6.

(8) Liu, H. Y.; Xu, S. M.; He, Z. M.; Deng, A. P.; Zhu, J. J. Supersandwich Cytosensor for Selective and Ultrasensitive Detection of Cancer Cells Using Aptamer-DNA Concatamer-Quantum Dots Probes. *Anal. Chem.* **2013**, *85* (6), 3385−3392.

(9) Chen, X. L.; Estevez, M. C.; Zhu, Z.; Huang, Y. F.; Chen, Y.; Wang, L.; Tan, W. H. Using Aptamer-Conjugated Fluorescence Resonance Energy Transfer Nanoparticles for Multiplexed Cancer Cell Monitoring. *Anal. Chem.* **2009**, *81* (16), 7009−7014.

(10) Wu, X.; Wu, M.; Zhao, J. L. X. J. Recent development of silica nanoparticles as delivery vectors for cancer imaging and therapy. *Nanomedicine* **2014**, *10* (2), 297−312.

(11) Song, Y.; Zhu, Z.; An, Y.; Zhang, W.; Zhang, H.; Liu, D.; Yu, C.; Duan, W.; Yang, C. J. Selection of DNA aptamers against epithelial cell adhesion molecule for cancer cell imaging and circulating tumor cell capture. *Anal. Chem.* **2013**, *85* (8), 4141−4149.

(12) Bi, S.; Ji, B.; Zhang, Z.; Zhang, S. A chemiluminescence imaging array for the detection of cancer cells by dual-aptamer recognition and bio-bar-code nanoprobe-based rolling circle amplification. *Chem. Commun. (Cambridge, U. K.)* **2013**, *49* (33), 3452−4.

(13) Zhao, J.; Zhu, L.; Guo, C.; Gao, T.; Zhu, X.; Li, G. A new electrochemical method for the detection of cancer cells based on small molecule-linked DNA. *Biosens. Bioelectron.* **2013**, *49*, 329−33.

(14) Chandra, P.; Noh, H. B.; Shim, Y. B. Cancer cell detection based on the interaction between an anticancer drug and cell membrane components. *Chem. Commun.* **2013**, *49* (19), 1900−1902.

(15) Zhu, Y.; Chandra, P.; Shim, Y.-B. Ultrasensitive and selective electrochemical diagnosis of breast cancer based on a hydrazine−Au nanoparticle−aptamer bioconjugate. *Anal. Chem.* **2013**, *85* (2), 1058−1064.

(16) Yan, M.; Sun, G. Q.; Liu, F.; Lu, J. J.; Yu, J. H.; Song, X. R. An aptasensor for sensitive detection of human breast cancer cells by using porous GO/Au composites and porous PtFe alloy as effective sensing platform and signal amplification labels. *Anal. Chim. Acta* **2013**, *798*, 33−39.

DOI: 10.1021/acsanm.9b01947
ACS Appl. Nano Mater. 2019, 2, 7421−7431

(17) Li, T.; Fan, Q.; Liu, T.; Zhu, X.; Zhao, J.; Li, G. Detection of breast cancer cells specially and accurately by an electrochemical method. *Biosens. Bioelectron.* **2010**, *25* (12), 2686−9.
(18) Mao, S.; Chang, J.; Zhou, G.; Chen, J. J. S. Nanomaterial-enabled Rapid Detection of Water Contaminants. *Small* **2015**, *11* (40), 5336−5359.
(19) Zhang, X.; Yin, J.; Yoon, J. Recent advances in development of chiral fluorescent and colorimetric sensors. *Chem. Rev.* **2014**, *114* (9), 4918−59.
(20) Zhang, X. Q.; Gong, S. W.; Zhang, Y.; Yang, T.; Wang, C. Y.; Gu, N. Prussian blue modified iron oxide magnetic nanoparticles and their high peroxidase-like activity. *J. Mater. Chem.* **2010**, *20* (24), 5110−5116.
(21) Gao, L.; Zhuang, J.; Nie, L.; Zhang, J.; Zhang, Y.; Gu, N.; Wang, T.; Feng, J.; Yang, D.; Perrett, S.; Yan, X. Intrinsic peroxidase-like activity of ferromagnetic nanoparticles. *Nat. Nanotechnol.* **2007**, *2* (9), 577−83.
(22) Masud, M. K.; Yadav, S.; Islam, M. N.; Nguyen, N. T.; Salomon, C.; Kline, R.; Alamri, H. R.; Alothman, Z. A.; Yamauchi, Y.; Hossain, M. S. A.; Shiddiky, M. J. A. Gold-Loaded Nanoporous Ferric Oxide Nanocubes with Peroxidase-Mimicking Activity for Electrocatalytic and Colorimetric Detection of Autoantibody. *Anal. Chem.* **2017**, *89* (20), 11005−11013.
(23) Chen, S.; Chi, M.; Yang, Z.; Gao, M.; Wang, C.; Lu, X. Carbon dots/Fe3O4 hybrid nanofibers as efficient peroxidase mimics for sensitive detection of H2O2 and ascorbic acid. *Inorg. Chem. Front.* **2017**, *4* (10), 1621−1627.
(24) Wang, Q.; Zhang, X.; Huang, L.; Zhang, Z.; Dong, S. interfaces, One-pot synthesis of Fe3O4 nanoparticle loaded 3D porous graphene nanocomposites with enhanced nanozyme activity for glucose detection. *ACS Appl. Mater. Interfaces* **2017**, *9* (8), 7465−7471.
(25) Kluenker, M.; Nawaz Tahir, M.; Ragg, R.; Korschelt, K.; Simon, P.; Gorelik, T. E.; Barton, B.; Shylin, S. I.; Panthofer, M.; Herzberger, J.; Frey, H.; Ksenofontov, V.; Möller, A.; Kolb, U.; Grin, J.; Tremel, W. Pd@Fe2O3 Superparticles with Enhanced Peroxidase Activity by Solution Phase Epitaxial Growth. *Chem. Mater.* **2017**, *29* (3), 1134−1146.
(26) Dong, Y.-l.; Zhang, H.-g.; Rahman, Z. U.; Su, L.; Chen, X.-j.; Hu, J.; Chen, X.-g. Graphene oxide−Fe 3 O 4 magnetic nanocomposites with peroxidase-like activity for colorimetric detection of glucose. *Nanoscale* **2012**, *4* (13), 3969−3976.
(27) Xu, H.; Shao, M.; Chen, T.; Zhuo, S.; Wen, C.; Peng, M. Magnetism-assisted assembled porous Fe3O4 nanoparticles and their electrochemistry for dopamine sensing. *Microporous Mesoporous Mater.* **2012**, *153*, 35−40.
(28) Lin, M.; Tan, H. R.; Tan, J. P. Y.; Bai, S. Understanding the growth mechanism of α-Fe2O3 nanoparticles through a controlled shape transformation. *J. Phys. Chem. C* **2013**, *117* (21), 11242−11250.
(29) Hu, M.; Korschelt, K.; Daniel, P.; Landfester, K.; Tremel, W.; Bannwarth, M. B.. Fibrous Nanozyme Dressings with Catalase-Like Activity for H2O2 Reduction To Promote Wound Healing. *ACS Appl. Mater. Interfaces* **2017**, *9* (43), 38024−38031.
(30) Annamalai, A.; Sandström, R.; Gracia-Espino, E.; Boulanger, N.; Boily, J.-F.; Mühlbacher, I.; Shchukarev, A.; Wågberg, T. Influence of Sb5+ as a Double Donor on Hematite (Fe3+) Photoanodes for Surface-Enhanced Photoelectrochemical Water Oxidation. *ACS Appl. Mater. Interfaces* **2018**, *10* (19), 16467−16473.
(31) Kim, C.-k.; Ghosh, P.; Rotello, V. M. Multimodal drug delivery using gold nanoparticles. *Nanoscale* **2009**, *1* (1), 61−67.
(32) Petrova, H.; Perez Juste, J.; Pastoriza-Santos, I.; Hartland, G. V.; Liz-Marzán, L. M.; Mulvaney, P. On the temperature stability of gold nanorods: comparison between thermal and ultrafast laser-induced heating. *Phys. Chem. Chem. Phys.* **2006**, *8* (7), 814−821.
(33) Kelemen, L. E. The role of folate receptor α in cancer development, progression and treatment: cause, consequence or innocent bystander? *Int. J. Cancer* **2006**, *119* (2), 243−250.
(34) Ritter, T. E.; Fajardo, O.; Matsue, H.; Anderson, R.; Lacey, S. W. Folate receptors targeted to clathrin-coated pits cannot regulate vitamin uptake. *Proc. Natl. Acad. Sci. U.S.A.* **1995**, *92* (9), 3824−3828.
(35) Sabharanjak, S.; Mayor, S. Folate receptor endocytosis and trafficking. *Adv. Drug Delivery Rev.* **2004**, *56* (8), 1099−1109.
(36) Boogerd, L. S.; Boonstra, M. C.; Beck, A.-J.; Charehbili, A.; Hoogstins, C. E.; Prevoo, H. A.; Singhal, S.; Low, P. S.; van de Velde, C. J.; Vahrmeijer, A. L. Concordance of folate receptor-α expression between biopsy, primary tumor and metastasis in breast cancer and lung cancer patients. *Oncotarget* **2016**, *7* (14), 17442.
(37) Liu, L.; Zhu, X.; Zhang, D.; Huang, J.; Li, G. An electrochemical method to detect folate receptor positive tumor cells. *Electrochem. Commun.* **2007**, *9* (10), 2547−2550.
(38) Xia, W.; Low, P. S. Folate-targeted therapies for cancer. *J. Med. Chem.* **2010**, *53* (19), 6811−6824.
(39) Zhang, L.-N.; Deng, H.-H.; Lin, F.-L.; Xu, X.-W.; Weng, S.-H.; Liu, A.-L.; Lin, X.-H.; Xia, X.-H.; Chen, W. In situ growth of porous platinum nanoparticles on graphene oxide for colorimetric detection of cancer cells. *Anal. Chem.* **2014**, *86* (5), 2711−2718.
(40) Low, P. S.; Antony, A. C. Folate receptor-targeted drugs for cancer and inflammatory diseases. *Adv. Drug Delivery Rev.* **2004**, *56* (8), 1055−1058.
(41) Coney, L. R.; Tomassetti, A.; Carayannopoulos, L.; Frasca, V.; Kamen, B. A.; Colnaghi, M. I.; Zurawski, V. R. Cloning of a tumor-associated antigen: MOv18 and MOv19 antibodies recognize a folate-binding protein. *Cancer Res.* **1991**, *51* (22), 6125−6132.
(42) Lu, Y.; Low, P. S. Folate-mediated delivery of macromolecular anticancer therapeutic agents. *Adv. Drug Delivery Rev.* **2012**, *64*, 342−352.
(43) Zhao, D.; Yu, G.; Tian, K.; Xu, C. Bioelectronics, A highly sensitive and stable electrochemical sensor for simultaneous detection towards ascorbic acid, dopamine, and uric acid based on the hierarchical nanoporous PtTi alloy. *Biosens. Bioelectron.* **2016**, *82*, 119−126.
(44) Sudimack, J.; Lee, R. J. Targeted drug delivery via the folate receptor. *Adv. Drug Delivery Rev.* **2000**, *41* (2), 147−162.
(45) Park, J.; An, K.; Hwang, Y.; Park, J.-G.; Noh, H.-J.; Kim, J.-Y.; Park, J.-H.; Hwang, N.-M.; Hyeon, T. Ultra-large-scale syntheses of monodisperse nanocrystals. *Nat. Mater.* **2004**, *3* (12), 891.
(46) Xu, Z.; Hou, Y.; Sun, S. Magnetic core/shell Fe3O4/Au and Fe3O4/Au/Ag nanoparticles with tunable plasmonic properties. *J. Am. Chem. Soc.* **2007**, *129* (28), 8698−8699.
(47) Laaksonen, T.; Ahonen, P.; Johans, C.; Kontturi, K. Stability and Electrostatics of Mercaptoundecanoic Acid-Capped Gold Nanoparticles with Varying Counterion Size. *ChemPhysChem* **2006**, *7* (10), 2143−2149.
(48) Vestal, C. R.; Zhang, Z. J. Atom transfer radical polymerization synthesis and magnetic characterization of MnFe2O4/polystyrene core/shell nanoparticles. *J. Am. Chem. Soc.* **2002**, *124* (48), 14312−14313.
(49) Yu, H.; Chen, M.; Rice, P. M.; Wang, S. X.; White, R.; Sun, S. Dumbbell-like bifunctional Au- Fe3O4 nanoparticles. *Nano Lett.* **2005**, *5* (2), 379−382.
(50) Daniel, M.-C.; Astruc, D. Gold nanoparticles: assembly, supramolecular chemistry, quantum-size-related properties, and applications toward biology, catalysis, and nanotechnology. *Chem. Rev.* **2004**, *104* (1), 293−346.
(51) Pang, L.-L.; Li, J.-S.; Jiang, J.-H.; Le, Y.; Shen, G. L.; Yu, R.-Q. A novel detection method for DNA point mutation using QCM based on Fe3O4/Au core/shell nanoparticle and DNA ligase reaction. *Sens. Actuators, B* **2007**, *127* (2), 311−316.
(52) Neeves, A. E.; Birnboim, M. H. Composite structures for the enhancement of nonlinear-optical susceptibility. *J. Opt. Soc. Am. B* **1989**, *6* (4), 787−796.
(53) Ye, X.; Shi, H.; He, X.; Wang, K.; He, D.; Yan, L. a.; Xu, F.; Lei, Y.; Tang, J.; Yu, Y. Iodide-responsive Cu−Au nanoparticle-based colorimetric platform for ultrasensitive detection of target cancer cells. *Anal. Chem.* **2015**, *87* (14), 7141−7147.
(54) Lu, W.; Arumugam, S. R.; Senapati, D.; Singh, A. K.; Arbneshi, T.; Khan, S. A.; Yu, H.; Ray, P. C. Multifunctional oval-shaped gold-nanoparticle-based selective detection of breast cancer cells using

DOI: 10.1021/acsanm.9b01947
ACS Appl. Nano Mater. 2019, 2, 7421−7431

simple colorimetric and highly sensitive two-photon scattering assay. *ACS Nano* **2010**, *4* (3), 1739−1749.
(55) Zhu, X.; Cao, Y.; Liang, Z.; Li, G. Aptamer-based and DNAzyme-linked colorimetric detection of cancer cells. *Protein Cell* **2010**, *1* (9), 842−846.
(56) Zhang, X.; Xiao, K.; Cheng, L.; Chen, H.; Liu, B.; Zhang, S.; Kong, J. Visual and highly sensitive detection of cancer cells by a colorimetric aptasensor based on cell-triggered cyclic enzymatic signal amplification. *Anal. Chem.* **2014**, *86* (11), 5567−5572.
(57) Tao, Y.; Lin, Y.; Huang, Z.; Ren, J.; Qu, X. Incorporating Graphene Oxide and Gold Nanoclusters: A Synergistic Catalyst with Surprisingly High Peroxidase-Like Activity Over a Broad pH Range and its Application for Cancer Cell Detection. *Adv. Mater.* **2013**, *25* (18), 2594−2599.
(58) Chen, H.; Dong, B.; Tang, Y.; Lin, W. Construction of a Near-Infrared Fluorescent Turn-On Probe for Selenol and Its Bioimaging Application in Living Animals. *Chem. - Eur. J.* **2015**, *21* (33), 11696−11700.
(59) Hevia, D.; Sainz, R. M.; Blanco, D.; Quirós, I.; Tan, D. X.; Rodríguez, C.; Mayo, J. C. Melatonin uptake in prostate cancer cells: intracellular transport versus simple passive diffusion. *J. Pineal Res.* **2008**, *45* (3), 247−257.
(60) Parker, N.; Turk, M. J.; Westrick, E.; Lewis, J. D.; Low, P. S.; Leamon, C. P. Folate receptor expression in carcinomas and normal tissues determined by a quantitative radioligand binding assay. *Anal. Biochem.* **2005**, *338* (2), 284−293.

DOI: 10.1021/acsanm.9b01947
ACS Appl. Nano Mater. 2019, 2, 7421−7431